

Quantifying daily NO_x and CO₂ emissions from Wuhan using satellite observations from TROPOMI and OCO-2

Qianqian Zhang^{1,2}, K. Folkert Boersma^{1,3}, Bin Zhao⁴, Henk Eskes³, Cuihong Chen⁵, Haotian Zheng⁴, Xingying Zhang²

5 ¹ Wageningen University, Environmental Science Group, Wageningen, the Netherlands

² Key Laboratory of Radiometric Calibration and Validation for Environmental Satellites, Innovation Center for Fengyun Meteorological Satellite (FYSIC), National Satellite Meteorological Center, China Meteorology Administration, Beijing, 100081, China

³ Royal Netherlands Meteorological Institute, De Bilt, the Netherlands

10 ⁴ State Key Joint Laboratory of Environmental Simulation and Pollution Control, School of environment, Tsinghua University, Beijing 100084, China

⁵ Satellite Application Center for Ecology and Environment, Ministry of Ecology and Environment of the People's Republic of China, Beijing, 100094, China

15 *Correspondence to:* K. Folkert Boersma, folkert.boersma@wur.nl, Qianqian Zhang, zhangqq@cma.gov.cn

Abstract. Quantification and control of NO_x and CO₂ emissions are essential across the world to limit adverse climate change and improve air quality. We present a new top-down method, an improved superposition column model to estimate day-to-day NO_x and CO₂ emissions from the large city of Wuhan, China, located in a polluted background. The latest released version 2.3.1 TROPOMI NO₂ columns and version 10r of the OCO-2 observed CO₂ mixing ratio are employed. We quantified daily NO_x and CO₂ emissions from Wuhan between September 2019 to October 2020 with an uncertainty of 31 % and 43 %, comparing to the 39% and 49% with the earlier v1.3 TROPOMI data, respectively. Our estimated NO_x and CO₂ emissions are verified against bottom-up inventories with minor deviations (< 3 % for the 2019 mean, ranging from -20 % to 48 % on a daily basis). Based on the estimated CO₂ emissions, we also predicted daily CO₂ column mixing ratio enhancements, which match well with OCO-2 observations (< 5 % bias, within ±0.3 ppm). We capture the day-to-day variation of NO_x and CO₂ emissions from Wuhan in 2019–2020, which does not reveal a substantial ‘weekend reduction’ but does show a clear ‘holiday reduction’ in the NO_x and CO₂ emissions. Our method also quantifies the abrupt decrease and slow NO_x and CO₂ emissions rebound due to the Wuhan lockdown in early 2020. This work demonstrates the improved superposition model to be a promising new tool for the quantification of city NO_x and CO₂ emissions, allowing policymakers to gain real-time information into spatial-temporal emission patterns and the effectiveness of carbon and nitrogen regulation in urban environments.

35 1 Introduction

Fossil fuel combustion by power plants, industrial activities, transportation, and residential energy use sectors leads to the emission of nitrogen oxides ($\text{NO}_x = \text{NO} + \text{NO}_2$) as well as carbon dioxide (CO_2). Traditional bottom-up NO_x and CO_2 emission estimates have a lag in time of several years because it takes time to access and compile accurate information on energy consumption and emission factors (Lamsal et al., 2011; Liu et al., 2020a).

40 For decades satellites have been continuously providing information on NO_2 distributions and trends with good quality, and satellite data is widely used to quantify NO_x emissions and changes (Lamsal et al., 2010; Visser et al., 2019; Zhang et al., 2020; Zhang et al., 2021). Based on satellite-retrieved NO_2 data, previous studies quantified long-term mean (monthly, yearly or multi-yearly) NO_x emissions on global and regional scales (Lamsal et al., 2011; Visser et al., 2019). Beirle et al. (2011) analyzed plumes of satellite NO_2 columns downwind of strong sources averaged for each wind direction and then inferred NO_x emissions from isolated significant point sources and megacities. Inspired by this idea, Lorente et al. (2019) analyzed the increase of NO_2 along with the wind over the extensive pollution source of Paris. The build-up of NO_2 over the city observed from space, in combination with wind speed and direction information, allows us to obtain day-by-day (sub-)urban NO_x emission estimates and lifetimes as long as the city is under a clear sky and winds are relatively constant in time. This approach does not need burdensome inverse modeling computations and opens possibilities for rapid and direct monitoring of NO_x emissions from space.

In contrast to NO_x , it is challenging to infer accurate localized anthropogenic CO_2 emissions from satellite CO_2 retrievals. One reason is that the background CO_2 concentration is orders of magnitude higher than the enhancement caused by anthropogenic emissions, reflecting the long atmospheric lifetime of CO_2 (Reuter et al., 2014; 2019). Another reason is that the spatial and temporal coverage of current CO_2 sensors is too sparse to allow substantial averaging of noisy signals by revisiting of scenes, precluding detailed CO_2 emission estimation (Zheng et al., 2020a; Liu et al., 2020a). Using satellite NO_2 measurements to estimate anthropogenic NO_x emissions as the basis to infer anthropogenic CO_2 emission has been proposed in several studies (Reuter et al., 2019; Liu et al., 2020a; Berezin et al., 2013; Zheng et al., 2020a). However, to our knowledge, there is no method that estimates day-to-day top-down CO_2 emission estimation on a (sub-)city scale.

Here we revisit the method of Lorente et al. (2019) to improve our understanding of its potential and limitations and extend it to estimate city-scale daily NO_x and CO_2 emissions. We present an improved superposition model that considers the build-up of pollution over a source area as in Lorente et al. (2019), as well as the decay of NO_2 downwind of the source, but now also accounts for changes in the background NO_2 pollution along the wind direction. The background NO_2 pollution was considered to remain constant by Lorente et al. (2019) for Paris, which is not surrounded by significant surface sources of NO_x pollution. Here we apply our improved method to a highly polluted urban area, the megacity of Wuhan in the Hubei Province of China, which, other than the relatively isolated city of Paris, is located in a polluted background with many surrounding

surface pollution sources that potentially interfere with the build-up and decay of the NO₂ plume from Wuhan. Using this improved superposition model, together with bottom-up information on the CO₂-to-NO_x emission ratio, we infer NO_x and CO₂ emissions on a day-by-day basis over a full year from September 2019 to August 2020 and analyze the variation in emissions and NO_x chemical lifetime from day to day. Of particular interest are the reductions and subsequent rebound of NO_x and CO₂ emissions associated with the COVID-19 lockdown measures in Wuhan, which have been reported in other studies, and serve here as a useful check on the robustness of our method.

2 Data and Material

2.1 Satellite data

In this study, we use the newly released level-2, version 2.3.1 of the S-5P TROPOMI data (TROPOMI-v2.3.1) between September 2019 to August 2020. The S-5P (Sentinel-5 Precursor) satellite was launched in October 2017 and the TROPOMI (TROPOspheric Monitoring Instrument) on board provides tropospheric NO₂ columns with an unprecedented horizontal resolution of up to 5.5 km × 3.5 km (as of 6 August 2019) and high signal-to-noise ratio (Griffin et al., 2019; Van Geffen et al., 2020). The v2.3.1 dataset is provided by S5P-PAL (S5P Science and Technology Product Algorithm Laboratory) (Eskes et al., 2021). It is dedicated to support the research on the impact of the COVID lockdown on air quality. Improved (residual) cloud pressures correct the low bias of v1.x data compared to OMI and ground-based measurements over east China (Wang et al., 2020; Liu et al., 2020b). In addition, improved treatment for the surface albedo increases the columns for cloud-free scenes (Van Geffen et al., 2022). Overall, compared to the earlier version, this dataset has 10–40 % higher tropospheric NO₂ columns over polluted scenes due to the improved cloud retrieval and other algorithm updates (Van Geffen et al., 2022; Riess et al., 2022). Over Wuhan, we find an average increase (compared to the v1.3 data, from now on referred to as TROPOMI-v1.3) in tropospheric NO₂ column density of about 25 %. Still, there are also differences between the two versions in terms of spatial and temporal distribution (Fig. S1). According to Fig. S1, the increase in v2.3.1 is much stronger over the polluted area (city center) and in the polluted period (9 September and 3 October 2019). Since the v1.x TROPOMI data is widely used in previous studies (e.g., Bauwens et al., 2020; Ding et al., 2020; Zhang et al., 2021), we also compared the estimated NO_x lifetime and emissions from the TROPOMI-v2.3.1 data and the TROPOMI-v1.3 data, which will be discussed in Sec. 3.1. For the record, when estimating the NO_x emissions and lifetime over Wuhan, we scaled up the TROPOMI-v1.3 NO₂ columns by a factor of 1.6 to correct for the known -40 % bias in TROPOMI NO₂ data as reported by Liu et al. (2020b).

We sampled the TROPOMI NO₂ columns into 0.05° latitude × 0.05° longitude grid cells (~ 6 × 6 km²). To ensure good data quality, we filtered out the data with cloud radiance fractions greater than 0.5 (geometric cloud fraction less than 0.2) and obtained 81 clear-sky days with full TROPOMI NO₂ coverage over the Wuhan region in one full year.

The column-averaged dry air mole fraction of CO₂ (XCO₂) data provided by the Orbiting Carbon Observatory-2 (OCO-2) is also employed to verify Wuhan's derived CO₂ emission inventory. We use version 10r of the bias-corrected XCO₂ product

(Gunson M and Eldering, 2020). The v10r OCO-2 XCO₂ product has high accuracy with single sounding precision of ~0.8 ppm over land and ~0.5 ppm over water and RMS biases of 0.5–0.7 ppm over both land and water (Odell et al., 2021).

2.2 Bottom-up emission information

100 Bottom-up NO_x and CO₂ emission inventories are used to provide the first guess of NO_x emission spatial pattern (for NO_x, in the Supplement Material, Text S1 and Fig. S2) and to verify the top-down emissions. We use the Air Benefit and Attainment and Cost Assessment System Emission Inventory (ABACAS) (Zhao et al., 2013; Zhao et al., 2018; Zheng et al., 2019) to provide NO_x and CO₂ emissions for the year 2019. The Multi-resolution Emission Inventory (MEIC) (Li et al., 2017) NO_x emissions for 2017 are also employed.

105 2.3 Other input data

Besides the satellite data and bottom-up emission inventories, a set of other parameters is input into our improved superposition model. They include the hydroxyl radical (OH) concentration, the loss rate (k) of NO_x in the atmosphere, the $\frac{[NO_x]}{[NO_2]}$ ratio, and the wind field. We use version 12.1 of the GEOS-Chem model with a horizontal resolution of $0.25^\circ \times 0.3125^\circ$ ($\sim 30 \times 37.5$ km²) to provide the a priori guesses for chemical parameters relevant to daytime NO_x. The wind field is from ERA5
110 (ECMWF Reanalysis v5), the fifth generation ECMWF (European Centre for Medium-Range Weather Forecasts) atmospheric reanalysis of the global climate (Hersbach et al., 2020). Detailed information on these data can be found in Text S2. Considering that the wind field strongly influences the distribution of NO₂ column patterns, and thus on the NO_x emission estimation, we filter the TROPOMI NO₂ data based on the wind fields. After excluding the days with fluctuating wind direction (if the wind direction changes more than 45 degrees in the hours before the TROPOMI overpass) within the study domain, we
115 finally obtained 50 days out of the ensemble of 81 valid satellite days between 1 September 2019 to 31 August 2020 to estimate NO_x and CO₂ emissions from Wuhan. The fraction of useful days is comparable to what Lorente et al. (2019) obtained for Paris, which is 27 days in 5 months.

2.4 NO₂ pattern fits: estimation of lifetime and emission

To ensure that the whole area of Wuhan is included, we determine our study domain as a circular region centered at 114° E,
120 30.7° N, with a diameter of ~186 km. It includes the whole area of Wuhan and the small city of Ezhou to the east of Wuhan, the southwest part of Huanggang, and the east part of Xiaogan (Fig. S4, the red circle). We also do a sensitivity test to narrow the study area down to within the Third Ring Road of Wuhan to check the robustness of our model to the area size of the study domain (Fig. S4, the blue circle). For each day, we converted the two-dimensional NO₂ column map over the domain to a one-dimensional line density along the wind direction (Text S3) (Beirle, 2011; Lorente et al., 2019). NO_x emissions and lifetimes
125 can be estimated by fitting the NO₂ line density over the domain.

Lorente et al. (2019) presented a superposition column model based on a simple column model (Jacob, 1999) to simulate NO₂ line density over Paris. They considered the build-up of NO₂ caused by spatially varying NO_x emissions from each cell and used the NO₂ line density value at the upwind end of the city to represent the background value, which they assumed to be constant over the city. This appears plausible if the background value would mostly represent free tropospheric NO₂ which has a longer lifetime than NO₂ in the oxidizing polluted boundary layer and varies smoothly according to models. Our method to simulate the NO₂ line density over the city is also based on the column model (Jacob, 1999) but differs from that of Lorente et al. (2019) in considering the background NO₂ value. Each cell along the wind direction is treated separately as a column model. Since the satellite overpasses at around 13:30 local time, NO_x is removed in the atmosphere dominantly through the first-order reaction with OH. NO_x emissions from the current cell contribute to the total line density through the build-up of NO₂ density within the cell and exponential decay of NO₂ downwind of the cell (Eq. (1)). It doesn't contribute to the upwind cells (Eq. (2)).

$$N_i(x) = \frac{E_i}{k} \left(1 - e^{-kL/u}\right) \times e^{-k(x-x_i)/u} \times \frac{[NO_2]}{[NO_x]} \quad \text{for } x > x_i, \quad (1)$$

$$N_i(x) = 0 \quad \text{for } x \leq x_i, \quad (2)$$

where N_i represents the NO₂ line density (molec cm⁻¹) contributed from E_i in cell i , L is the length of each cell, i.e. 600000 cm; k is the loss rate (s⁻¹) of NO_x at 13:00 local time ($k = \frac{k'[OH]}{[NO_x]/[NO_2]}$); and u denotes the NO₂-density-weighted mean wind speed in unit of cm s⁻¹ within planet boundary. We add up the contributions from each cell and the background value to model the overall NO₂ line density:

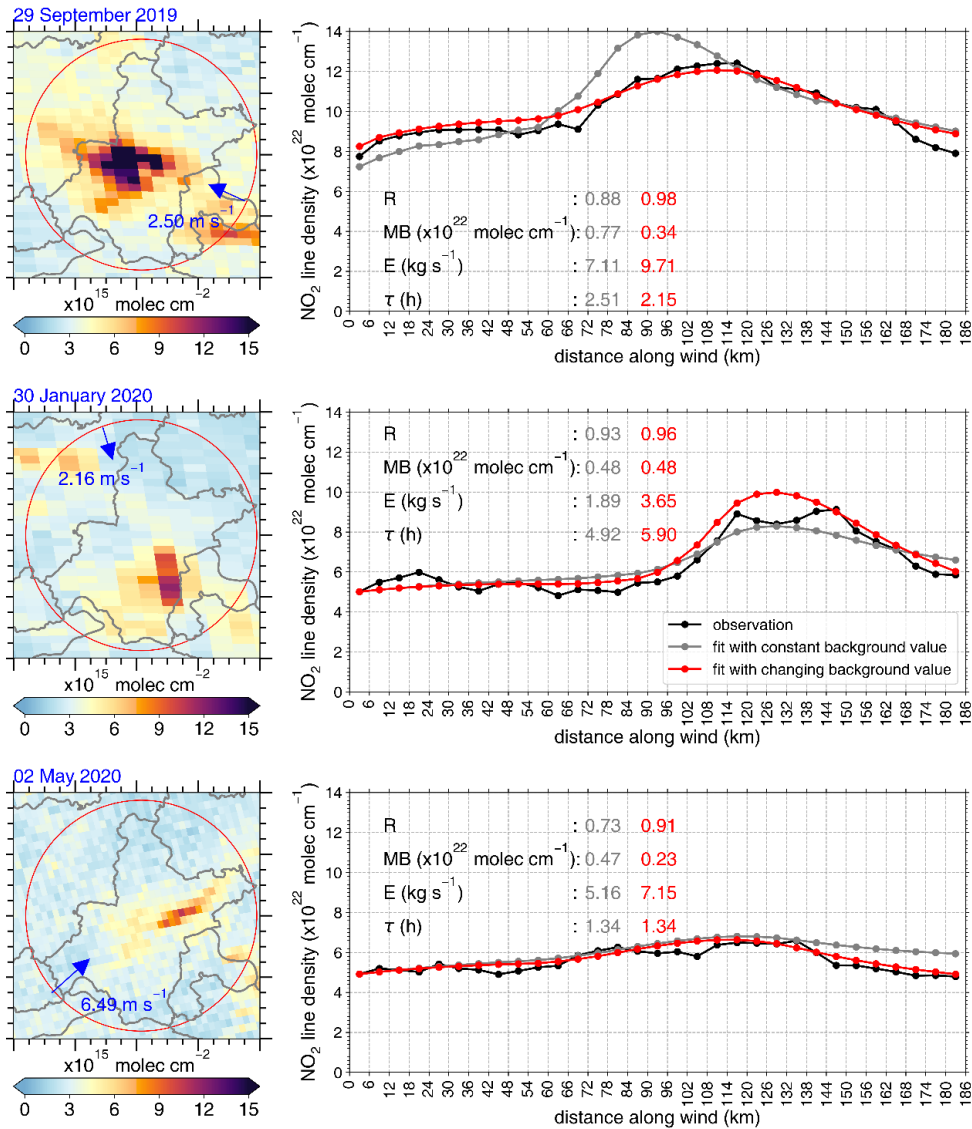
$$N(x) = \sum_{i=1}^n N_i(x) + b + \alpha x. \quad (3)$$

Here, b represents the starting background value, equivalent to the mean NO₂ line density within the 5 (for summer, spring, and autumn) or 10 (for winter) cells upwind of $x=0$. α denotes the linear change of background value with distance along the wind and represents the chemical decay of background NO₂ flowing into the polluted boundary layer over the city.

We fit the terms that drive $N(x)$ (i.e. E_i , k and α) with the fixed L , u and $\frac{[NO_x]}{[NO_2]}$ from external data, via a least-squares minimization to the TROPOMI observed line density $N_{TROPOMI}(x)$. For each day, we run the model 20 times randomly choosing OH concentration within the $\pm 20\%$ interval of the GEOS-Chem simulated OH concentration. The set of parameters E_i , k and α that best explain the observations over the city is the answer we are seeking for. The parameter that describes the decay of upwind NO₂ over the city, the α value, is determined by the difference of NO₂ line density between the end and start point of the study domain, $\alpha = \frac{(N_{31} - N_1)}{30L}$, and we allow it to change between $\pm \alpha$ in the fitting procedure. For the 50 days on average, the α value is $(-0.006 \pm 0.008) \times 10^{-22} \text{ molec cm}^{-2}$. The α value being negative reflects the decay of upwind NO₂ pollution along the wind.

155 The assumption of a linearly decreasing NO_2 background is relevant under conditions when the city is in a polluted background. It accounts for decay of upwind NO_2 pollution arriving at the city when transported over and downwind of the city. In reality, upwind NO_2 pollution mixes in with the freshly emitted NO_x and is then subject to chemical decay (with non-linearities due to turbulent mixing and spatial heterogeneity in emissions). We acknowledge that our linear decrease of background NO_2 pollution is a severe simplification. Still, as shown in Fig. 1, compared to fitting results with a constant background value, we obtain a better correlation (up to 25%) and lower bias (nearly 50% lower) between fitted and observed NO_2 line densities when fitting with a linearly changing background value.

160



165 **Figure 1: Tropospheric NO₂ columns over Wuhan on 29 September 2019, 30 January 2020 and 2 May 2020 (left, from top to bottom), the red circle inside each map defines the study domain. The corresponding NO₂ line densities along wind within the study domain are given in the right panel. For each day, the correlation coefficient (R) between the observed (black line) and fitted (grey and red lines) NO₂ line density are given. The fitted mean bias (MB), NO_x emissions (E) and NO_x lifetime (τ) are also displayed.**

2.5 CO₂ emission estimation

City-scale CO₂ emissions are estimated through Eq. (4):

$$170 E_{CO_2} = E_{NO_x} \times Ratio_{CO_2-to-NO_x}, \quad (4)$$

The anthropogenic CO₂-to-NO_x emission ratio is provided by the ABACAS inventory and amounts to ~591 gCO₂/gNO_x emitted from our study domain for the year 2019. In 2020, emissions from the transport sector had substantially decreased due to the lockdown measurements (Huang et al., 2021; Zheng et al., 2020c). The more substantial decrease in transport NO_x emissions relative to declines from other sectors is predicted to have led to an increase in the CO₂-to-NO_x emission ratio, for this ratio is lowest in the transport sector (Zheng et al., 2020c). The monthly CO₂-to-NO_x emission ratio for Wuhan was calculated based on recent reports on sectoral NO_x emissions in 2020 from Hubei Province (Zheng et al., 2021a). We further calculated the daily CO₂-to-NO_x emission ratio based on the monthly, daily, and diurnal variations of CO₂ and NO_x emissions (Fig. S5). The final daily CO₂-to-NO_x emission ratio for the study period displayed in Table S1 indeed shows increases in the CO₂-to-NO_x emission ratio of up to 20 % during the lockdown period in 2020 due to the reduced contribution from the transport
180 sector.

2.6 Uncertainty in NO_x and CO₂ emission estimation

Uncertainties in quantifying NO_x and CO₂ emissions contain the systematic error in the TROPOMI NO₂ retrieval, bias in the assumed a priori OH concentration, NO_x/NO₂ ratio, CO₂-to-NO_x emission ratio, uncertainties in wind fields, and the area of study domain. The v2.3.1 NO₂ column dataset corrected the low bias in TROPOMI (v1.x) tropospheric NO₂ column over
185 Eastern China by 15–100 % (Van Geffen et al., 2022), but there remains an uncertainty of ~ ±20 %. The CTMs have difficulty simulating accurate OH concentration, but for > 90 % of the days, our fitted OH concentrations fall in the ±20 % range around GEOS-Chem simulation, so the uncertainty in OH concentration is likely on the order of ±20 %. The difference between the model simulated and observed NO_x/NO₂ ratio is less than 10 %, so we give an uncertainty in NO_x/NO₂ ratio of ±10 %. Uncertainty in the CO₂-to-NO_x emission ratio comes from the errors in sectoral NO_x and CO₂ emissions, and we calculated
190 that the corresponding uncertainty is ±30 %. We use the NO₂-column-weighted mean instead of the arithmetic mean value to get the boundary layer mean wind speed to minimize the error in the wind field, but there may remain ±20 % uncertainty in the ERA5 reanalysis data. We ran a test by randomly choosing parameter values within their uncertainty ranges 20 times to predict an ensemble of NO_x and CO₂ emission outcomes. Then the ratio of the standard deviation to the mean value of the 20 emission outcomes is regarded as the uncertainty on NO_x and CO₂ emission caused by uncertainties in the corresponding

195 parameters, which are displayed in Table S2. The uncertainty caused by the domain size is determined by narrowing down our study domain to the Wuhan city center (see Text S4 and Fig. S6). The results demonstrate that when the study domain is narrowed down to 84 km diameter, as expected, it turns out to be structurally different from that with the 186 km diameter domain. This is because that the mean OH concentration is lower in the city center, leading to longer fitted NO_x lifetime. However, the change in fitted NO_x lifetime and NO_x emission is within $\pm 15\%$. So, we give a 15% uncertainty in NO_x emissions and lifetime estimation caused by the size in the areas of the study domain. Finally, considering that all these parameters are independent of each other, we use the root mean square sum of the contributions to represent the overall uncertainty estimation, which we quantify for NO_x emission on a single day at $\sim 31\%$, and for CO_2 emission at $\sim 43\%$.

3 Results and discussion

3.1 NO_x Lifetimes and emissions

205 We display the estimated NO_x lifetime and NO_x emissions for each clear-sky day during the study period in Table S1. The estimated planetary boundary layer mean OH concentration over the region for each day is presented in Fig. 2. For 90 % of the days, our model fitted OH concentrations fall into the intervals of $0.8\sim 1.2\times$ the GEOS-Chem model values. There are only 5 days on which we had to impose a change in OH concentrations of more than 30 % relative to the GEOS-Chem simulation to obtain realistic fitting results.

210

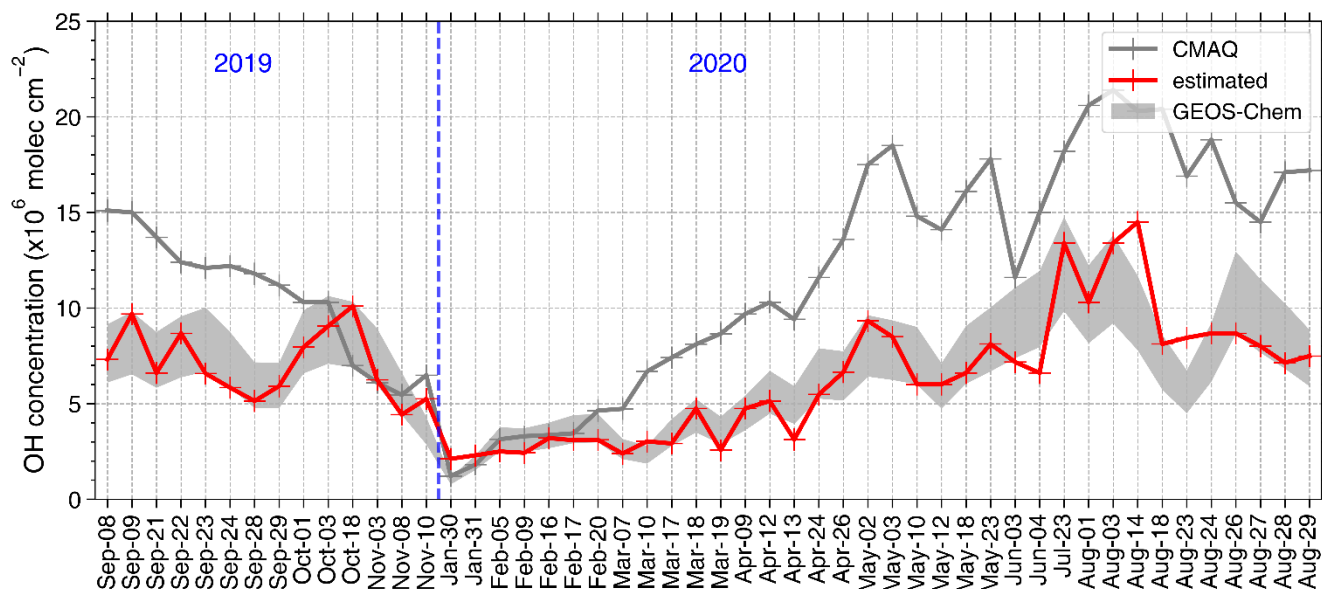


Figure 2: Daily boundary layer mean OH concentration over our study domain. The OH concentration estimated from our improved superposition column model is given with the red line. The grey shade represents 0.8–1.2 times GEOS-Chem simulated OH concentration, and the grey line represents CMAQ model simulation results.

215 We estimate that the seasonal mean noontime NO_x lifetime over Wuhan and adjacent region is 4.8 ± 0.8 h for winter, 2.8 ± 1.3
h for spring, 1.4 ± 0.3 h for summer, and 1.9 ± 0.5 h for autumn. The results are lower than those calculated from the GEOS-
Chem simulation by Shah et al. (2020), with ~ 6 h in summer and >20 h in winter. This is because they figured the 24-hour
mean NO_x lifetime while the loss rate of NO_x is much higher around noon. NO_x lifetime for Wuhan is also shorter than for
Paris (Lorente et al., 2019), especially during winter, reflecting the higher radiation levels and temperature in Wuhan than in
220 Paris. It should be noted that Liu et al. (2016) fitted a NO_x lifetime of 2.6 h for Wuhan in the warm season (May to September)
for 2005–2013 mean, and our result for 2019–2020 is 1.7 ± 0.4 h. One reason is that they calculated NO_x lifetime based on a
long-term mean NO_2 distribution and the coarser resolution of OMI data, both of which lead to spatial smoothing of NO_2
gradients and thus longer apparent NO_x lifetimes (Qu, 2020). Another explanation is the increasing ozone concentrations in
China in recent years (Li et al., 2020) promotes OH formation and thereby NO_x loss reactions which shorten NO_x lifetime
225 (Zara et al., 2021).

The estimated NO_x lifetime and emissions from the two TROPOMI datasets for the whole study period are presented in Fig.
S7. On average, the TROPOMI-v1.3 data results in 13 % lower NO_x emissions from Wuhan than the TROPOMI-v2.3.1 data.
 NO_x lifetime estimated from TROPOMI-v1.3 data is 5 % shorter than that from TROPOMI-v2.3.1, which may be attributed
to the fact that the TROPOMI-v2.3.1 data has a higher gradient between the city center to the background. Uncertainties in
230 NO_x emissions and lifetime estimation are 33% higher in the TROPOMI-v1.3 data (39%) for the higher uncertainty in the NO_2
column data (here we use 30 %).

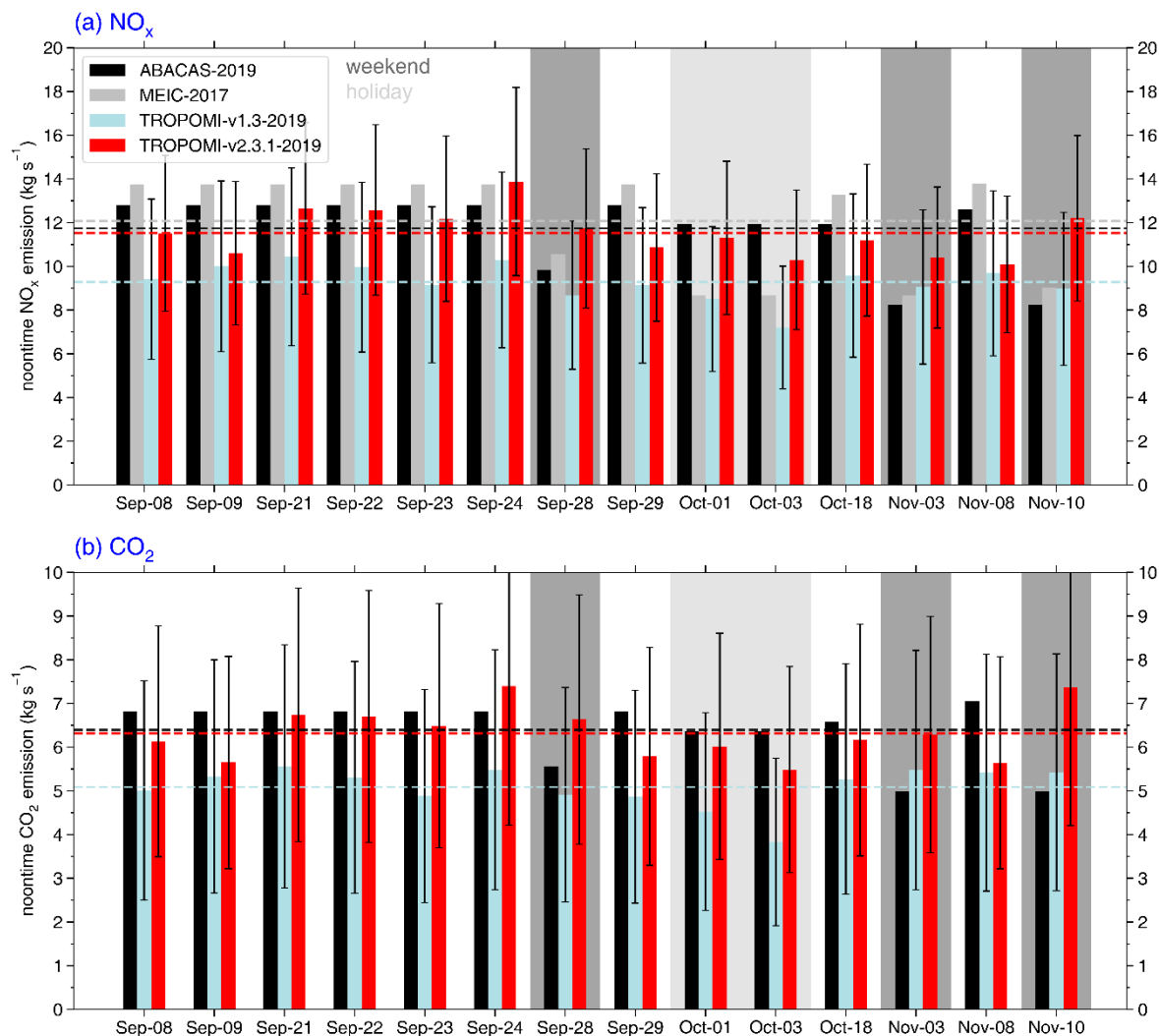


Figure 3: Daily noontime (a) NO_x and (b) CO₂ emissions in Wuhan estimated from TROPOMI (red and blue bars, the error bars represent the uncertainty in the emission estimations) and the bottom-up emission inventories ABACAS (black bars) for the year 2019 and MEIC (silver bars) for the year 2017. The dark and light grey shades represent weekends and holidays, respectively. The mean levels of each dataset are given as dashed lines with corresponding colors.

We further verified the estimated NO_x emissions from the two TROPOMI datasets in 2019 with the bottom-up emission inventories. We obtained 14 days (including 9 weekdays, 3 weekends, and 2 holidays) between September and November 2019 for the top-down NO_x emission estimation and compared them with those from the ABACAS (2019) and MEIC (2017) inventories. Overall, as presented in Fig. 3a, compared to the bottom-up emission inventories, TROPOMI-v1.3-2019 NO_x emissions are 21 % and 23 % lower than ABACAS-2019 and MEIC-2017, respectively. On the other hand, TROPOMI-v2.3.1-2019 NO_x emissions are comparable to those from ABACAS-2019 (2 % difference) and ~5 % lower than MEIC-2017. That

NO_x emissions estimated from TROPOMI-v2.3.1 in 2019 are lower than MEIC-2017 likely reflects the fact that NO_x emissions have decreased in 2019 relative to 2017 in response to Chinese emission controls. According to Wuhan Bureau of Statistics, NO_x emissions have reduced by 6 % between 2017 and 2019 (Statistics, 2019; Bauwens et al., 2020), close to the difference between TROPOMI-v2.3.1-2019 and MEIC-2017. Through the comparison with the bottom-up emissions, we find that the TROPOMI-v2.3.1 NO₂ data generates more reliable NO_x emissions from Wuhan in 2019 than the v1.3 data, even when the low bias in TROPOMI-v1.3 data is corrected by a factor of 1.6.

Unlike the bottom-up inventories, our daily TROPOMI NO_x emissions do not indicate the existence of a so-called ‘weekend reduction effect’ but do point out a distinct ‘holiday reduction effect’ in Wuhan NO_x emissions. The bottom-up inventories suggest that weekend NO_x emissions are 30 % reduced relative to weekdays. The TROPOMI-v2.3.1 estimation shows reductions in weekend NO_x emission of < 3 %, while on the two days (1 and 3 October) of the National Holiday, NO_x emissions are 8% lower than the workday mean. Surface NO₂ and O₃ observations from Beijing do not show a weekend effect (Zhao et al., 2019; Hua et al., 2021) either. Our TROPOMI top-down NO_x emissions show a similar spatial pattern as in the ABACAS and MEIC (Fig. S2), with the highest emissions located in the city center of Wuhan. However, the TROPOMI NO_x emission pattern appears more smeared-out NO_x than ABACAS due to the strong dependence of the bottom-up spatial distribution on population density, the difference in spatial resolution, and the decrease in NO_x emissions in early 2020, mainly occurring in the high-emission region.

3.2 CO₂ emissions and XCO₂ enhancements

We estimate noontime top-down (technically representing a merger of top-down and bottom-up information, but we define it as top-down for simplicity) CO₂ emissions from Wuhan between September and November 2019 to be $6.32 \pm 2.74 \text{ t s}^{-1}$ (the errors represent the uncertainty of the emission estimation), comparable to ABACAS-2019, of $6.40 \pm 2.78 \text{ t s}^{-1}$ (Fig. 3b). Based on the estimated daily CO₂ emissions, we further use the superposition column model to simulate daily XCO₂ enhancements and evaluate them with OCO-2 observations. We successfully obtained two days between May 2018 (start time of TROPOMI-v2.3.1 NO₂ product) and December 2021 with simultaneous (both overpass at around 13:00–13:30 local time), co-located TROPOMI NO₂ and OCO-2 CO₂ observations over Wuhan, 15 September 2018 and 13 April 2020. We inferred total top-down CO₂ emissions from Wuhan based on our TROPOMI-inferred NO_x emissions and the ABACAS-predicted CO₂-to-NO_x emission ratios on 15 September 2018 and 13 April 2020 to be $7.92 \pm 3.44 \text{ t s}^{-1}$ and $4.44 \pm 1.93 \text{ t s}^{-1}$, respectively. Then they are used to predict the XCO₂ enhancements with the superposition column model. To compare with the sparse distributed OCO-2 observations, we apply the superposition model on the CO₂ line density with 1km wide, while it is 186 km wide for NO₂. The column model doesn’t take the diffusion of NO₂ or CO₂ into account, but it can be assumed that all diffusion is encapsulated within the domain for a line density covering a cross-section as wide as 186 km. However, when the line density is only 1 km wide, the diffusion will move some CO₂ out of this line, and this will influence the CO₂ enhancement prediction. We will discuss this influence further below.

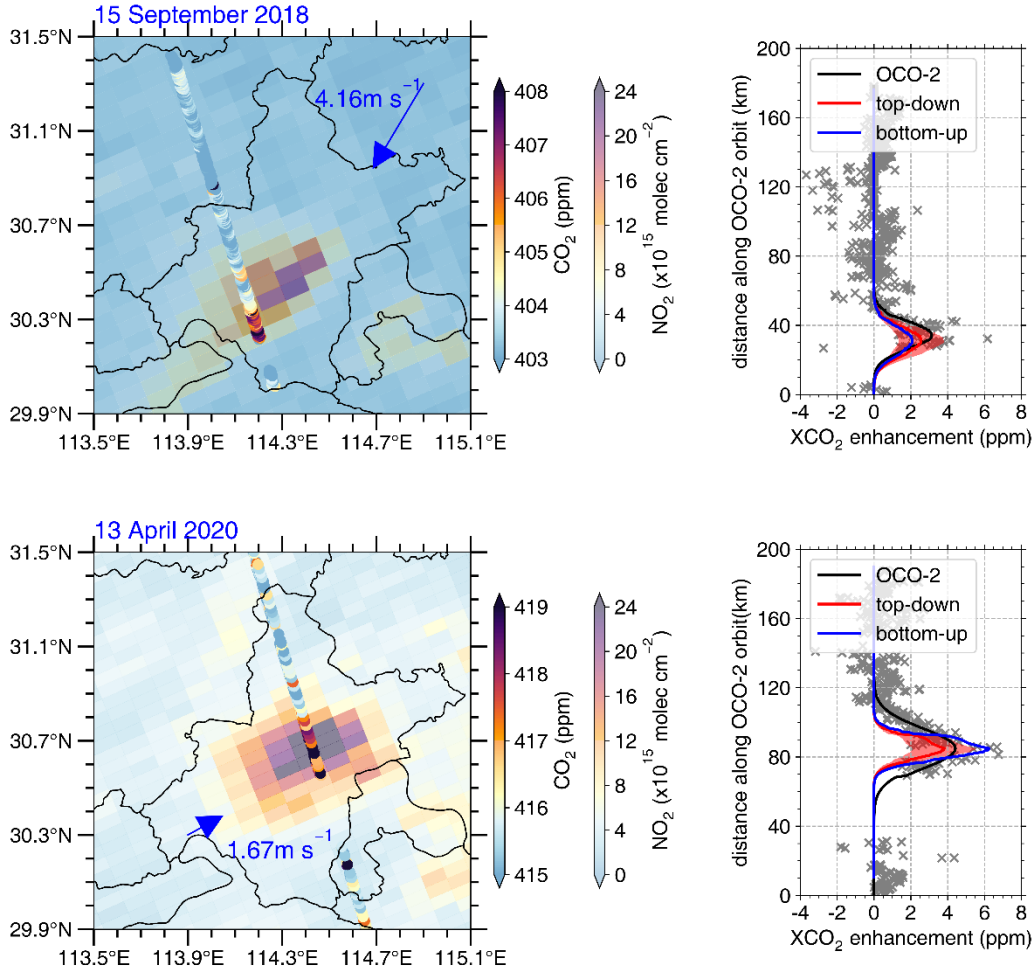
275 Neglecting chemical production and loss of CO_2 in the atmosphere, the superposition column model of CO_2 (Eq. 5) is simpler than that of NO_x :

$$N_{\text{CO}_2} = \frac{E_{\text{CO}_2}}{uL}, \quad (5)$$

here N_{CO_2} is CO_2 density in unit of g m^{-2} , E_{CO_2} denotes our estimated CO_2 emission (g s^{-1}), and u and L are the wind speed (m s^{-1}) and length of grid cell (6000 m). Then N_{CO_2} (g m^{-2}) is converted to the dry air column mixing ratio $X\text{CO}_2$ (ppm) to compare
 280 with the OCO-2 observation (Zheng et al., 2020a):

$$X\text{CO}_2 = N_{\text{CO}_2} \times \frac{M_{\text{air}}}{M_{\text{CO}_2}} \times \frac{g}{p-wg} \times 10^3, \quad (6)$$

in which M_{air} and M_{CO_2} are air and CO_2 molar mass of air and CO_2 (g mol^{-1}), g is the gravitational acceleration (9.8 m s^{-2}), p (Pa) and w (kg m^{-2}) are surface pressure and total column water vapor, respectively.

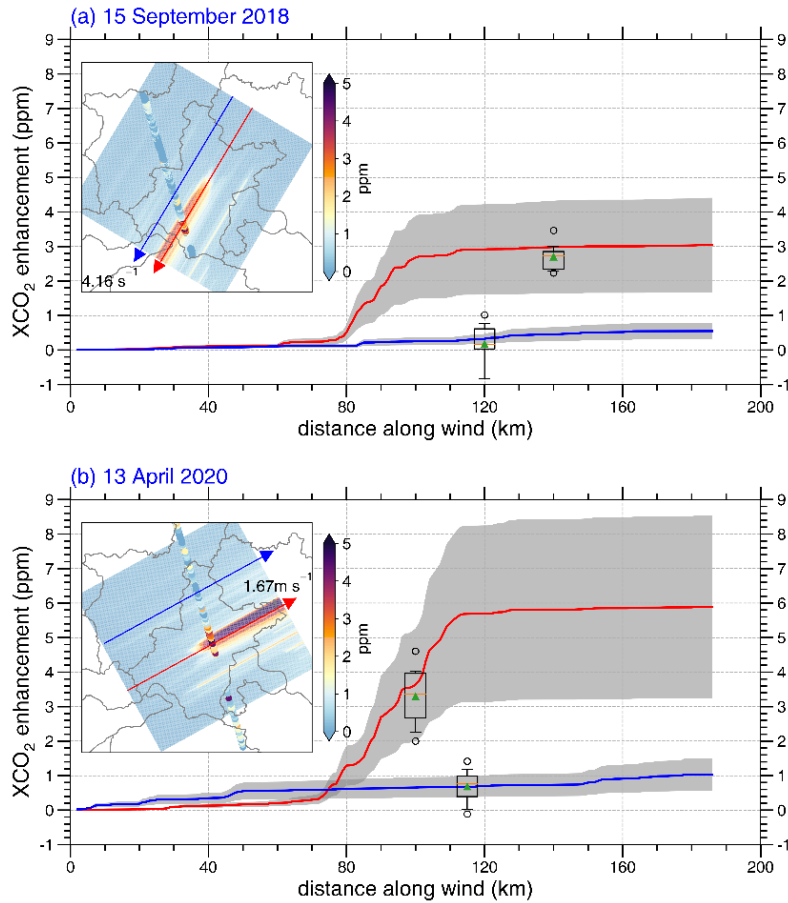


285 **Figure 4: Simultaneous, co-located TROPOMI NO₂ and OCO-2 CO₂ observations over Wuhan (the left panel) on 15 September 2018 (top) and 13 April 2020 (bottom), the wind speed and direction on each day are shown. The dry air mole fraction of CO₂ (XCO₂) enhancements along the OCO-2 orbit are given for the corresponding day (the right panel). The grey xs and black lines represent the OCO-2 observation. The blue lines denote XCO₂ enhancement predicted with bottom-up emissions, and the red lines (shading represents the uncertainty interval) with top-down CO₂ emission estimated in this study.**

290 We calculate the XCO₂ enhancement due to the top-down CO₂ emissions on 15 September 2018 and 13 April 2020 and compare these with the enhancements observed by OCO-2. As shown in the right panels of Fig. 4, the superposition model captures the spatial pattern of observed XCO₂ along the OCO-2 orbit on both days. The predicted amplitudes of the XCO₂ enhancements are also comparable to those in the OCO-2 observation with a small bias (less than 5 % for both days). For comparison, we also use the 2019 bottom-up CO₂ emissions to predict the XCO₂ enhancement on the two days (blue lines in
295 Fig. 4, the right panel). XCO₂ enhancements predicted by bottom-up CO₂ emissions deviate more from the OCO-2 observed enhancements than those predicted by the top-down CO₂ emissions. On 13 April 2020 in particular, the bottom-up enhancement differs by +41% while the top-down differs by only within ± 5 % compared to the observed XCO₂ enhancement. At the beginning of Wuhan's reopening, CO₂ emission from the city (our top-down estimation) is expected to be far lower than the pre-lockdown level (bottom-up estimation).

300 We see that the predicted XCO₂ enhancements on 13 April 2020, both from the bottom-up and top-down emissions, are much 'narrower' compared to the OCO-2 observation. On this day, the OCO-2 orbit passes over the city center, and the diffusion plays an important role, which is neglected in the column model. In contrast, on 15 September 2018, the OCO-2 orbit passed downwind of the city center, and the width of the predicted and observed XCO₂ enhancements are more comparable. For comparison, we also ran a Gaussian plume model to simulate the XCO₂ enhancement (Text S5 and Fig. S8). On 13 April
305 2020, the result from Gaussian model agrees better with the OCO-2 observation, and on 15 September 2018, results from the two models (Gaussian model and the superposition column model) are close to each other and match well with the observation.

We also display XCO₂ enhancement line densities along the wind direction with uncertainty on both days (Fig. 5). The line density shows a substantial increase of XCO₂ along the wind direction over the region with strong CO₂ emissions (Fig.5a, b, the inset maps). Where lines cross the OCO-2 orbit, the observed XCO₂ (as boxplots in Fig. 5a, b) are shown and their values
310 agree with the predicted XCO₂ lines within ± 0.3 ppm. It is remarkable that the XCO₂ enhancement is lower on 15 September 2018 than on 13 April 2020, despite CO₂ emission on 15 September 2018 being nearly 65 % higher than those on 13 April 2020. The main reason for this is the lower wind speed on 13 April 2020, which accumulates pollutants over the city, and the fact that OCO-2 ground-track passed over the city center of Wuhan on this day. On 15 September 2018, higher wind speeds and the OCO-2 track being situated over the outskirts of the city imply that a lower enhancement of CO₂ is observed.



315

Figure 5: Two presentative predicted XCO₂ enhancement lines (red and blue) with uncertainty (grey shades) on (a) 15 September 2018 and (b) 13 April 2020. When the XCO₂ enhancement lines pass through the OCO-2 orbit, the observed XCO₂ enhancements are shown with boxplots. The mean values are shown as green triangles, and the outliers beyond the 5–95 % interval are shown as circles. The predicted XCO₂ enhancement line density maps overlaid with OCO-2 observed XCO₂ enhancement on each day are shown inside, with the position of the presentative lines and the wind direction.

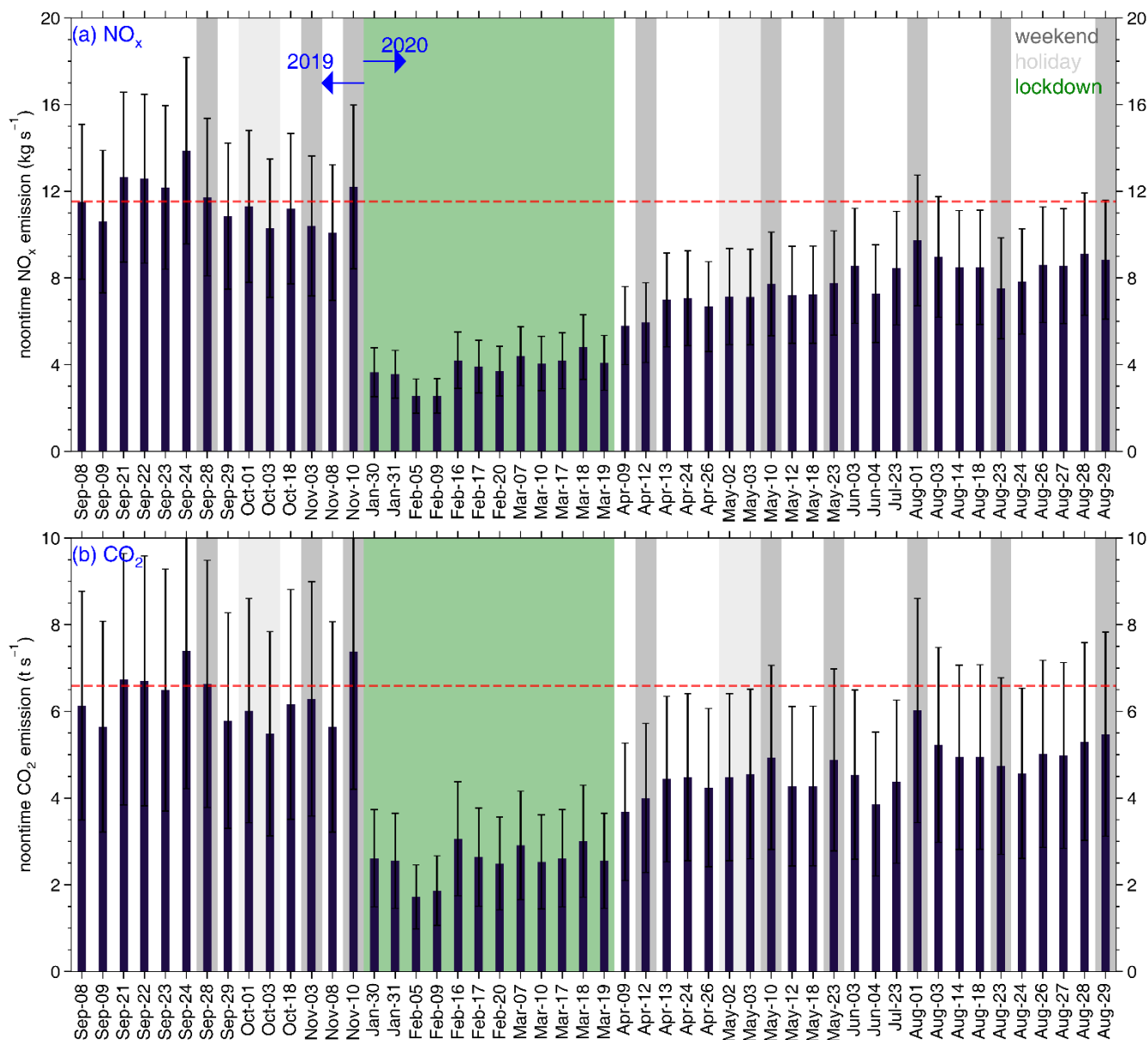
320

We use an ‘indirect’ method to estimate daily city anthropogenic CO₂ emissions and then predict XCO₂ enhancements, which may induce uncertainties from the NO_x emission estimation, the assumption of CO₂-to-NO_x emission ratio, and the model to predict XCO₂ enhancements. Despite all these uncertainties, we still generate daily Wuhan CO₂ emissions and XCO₂ enhancements that agree well with bottom-up inventory and OCO-2 observation, respectively.

325 3.3 Variation of NO_x and CO₂ emissions in Wuhan from September 2019 to August 2020

Figure 6 displays the day-to-day variation of NO_x and CO₂ emissions in Wuhan between September 2019 and August 2020. Before the pandemic of COVID-19, NO_x emissions stayed at a stable level of 11.53±1.08 kg s⁻¹, and CO₂ at 6.32±0.66 t s⁻¹

330 (the errors denote the standard deviation), as indicated by the dashed red lines. From January 2020 onwards, strict lockdown measurements were implemented to combat the COVID-19 pandemic, which led to lower industry production and less traffic on the road, and a sharp drop in NO_x and CO_2 emissions (Ding et al., 2020; Zhang et al., 2020; Zheng et al., 2021b; Zhang et al., 2021; Feng et al., 2020). Our method closely captures the timing and magnitude of these well-known sharp reductions in emissions.



335 **Figure 6: 50 days (a) NO_x and (b) CO₂ emissions in Wuhan estimated from TROPOMI between 1 September 2019 to 31 August 2020. The error bars denote the uncertainty in emission estimations, and the weekends, holidays, and lockdown period are shaded with dark grey, light grey, and green colors, respectively. The mean pre-lockdown emission levels are given as red dashed lines.**

Wuhan NO_x emissions on 30 January 2020 were $3.65 \pm 1.59 \text{ kg s}^{-1}$, nearly 70 % lower than pre-lockdown levels, and decreased further and came to the lowest level in early February 2020, in accordance with Feng et al. (2020) who estimated similar reductions based on surface NO₂ observations. 5 February is the day with our lowest NO_x emission from Wuhan of
340 $2.55 \pm 1.11 \text{ kg s}^{-1}$, only ~22 % of the normal level. CO₂ emissions have a similar temporal pattern as NO_x emissions, but the reduction relative to pre-lockdown level is smaller. The lowest CO₂ emission is at ~27 % of the pre-lockdown level (also on 5 February 2020), and the mean emission rate during the lockdown period (23 January to 8 April 2020) is 60 % lower than pre-lockdown level, while it is 67 % for NO_x. That CO₂ emission reductions are more modest than NO_x reductions, reflecting the fact that the transportation sector had the strongest reductions during the lockdown, but since this sector also has the lowest
345 CO₂-to-NO_x ratios, the relative reduction in CO₂ remains somewhat smaller than in NO_x emissions. This finding is similar to that of Zheng et al. (2020b), who estimated the NO_x and CO₂ emission variations for the whole China.

From early February 2020 onwards, emissions increased slowly throughout the lockdown period. Wuhan NO_x emissions intensity in February 2020 was no more than 4.20 kg s^{-1} , some 60 % below the pre-lockdown level. Feng et al. (2020) estimated 61 % lower NO_x emission from Wuhan in February 2020 than in January based on surface NO_x observations. Zheng et al.
350 (2021a) reported a ~50 % lower NO_x emission from Hubei province in February 2020 than the annual mean level estimated from a bottom-up approach.

Although Wuhan reopened on 9 April, the NO_x and CO₂ emissions did not see significant increases up until mid-May 2020. A perceptible increase in NO_x emission is seen during late May, climbing to $> 7.50 \text{ kg s}^{-1}$ (NO_x) and $> 4.5 \text{ t s}^{-1}$ (CO₂), and levelling off thereafter. In August 2020, Wuhan NO_x emissions were still some 25 % lower than the pre-lockdown level.
355 Although bottom-up estimation by Zheng et al. (2021a) suggested that NO_x emissions from the Hubei province were similar in May–August 2020 as in 2019, surface and satellite observations over Wuhan show a 15–20 % lower NO₂ concentrations in May–August 2020 compared to 2019 (Fig. S9 and S10), consistent with our estimation of NO_x emissions. Liu et al. (2020c) reported 4.8 % higher CO₂ emissions for the whole China in August 2020 compared to August 2019. For the city of Wuhan, however, we calculate here some 20 % lower CO₂ emissions in August 2020 compared to the pre-lockdown level. Wuhan
360 experienced a much more strict and longer period lockdown than other regions of China, and therefore a slower rebound of NO_x and CO₂ emissions should be expected.

As we have stated above, to ensure the performance of the model, we must filter out the days when cloud fraction is greater than 0.2 and the days when the wind direction shows substantial spatial or temporal variation within the study domain. Finally, we obtain 50 out of the 365 days with reliable NO_x and CO₂ emissions estimation. However, these 50 days cover at least 2
365 days for each month (except for December 2019). For 2019, it includes 9 workdays, 3 weekend days, and 2 holiday days, which are enough to investigate the ‘weekend reduction effect’ and ‘holiday reduction effect’ in NO_x emissions. It also covers

12 days across the lockdown period and 24 days after that, allowing us to monitor the large reduction and recovery of NO_x and CO₂ emissions from Wuhan due to the COVID lockdown. Therefore, these 50 days provide useful information to investigate the temporal emission patterns of NO_x and CO₂ from Wuhan and help to monitor the effectiveness of emission reductions in large urban centers.

4 Conclusion

In this study, we introduced an improved superposition column model to estimate daily NO_x and CO₂ emissions from a Chinese megacity of Wuhan based on the latest released version 2.3.1 of TROPOMI NO₂ column data and OCO-2 XCO₂ observation. Our estimated daily NO_x and CO₂ emissions agree well with bottom-up emissions with a small bias of < 3 %. Predicted XCO₂ enhancements based on our CO₂ emissions estimates are proved to be in good agreement (within ±5 %) with OCO-2 observations over Wuhan. Compared to previous studies, our work shows that satellite measurements can provide detailed information on sub-city scale NO_x and CO₂ emissions on a daily basis. We achieved the day-to-day variation of NO_x and CO₂ emissions from Wuhan between September 2019 and August 2020. We pointed out that the ‘weekend reduction effect’ is small, but a ‘holiday reduction effect’ in Wuhan NO_x and CO₂ emissions can be clearly detected. We also captured the abrupt decrease in NO_x and CO₂ emissions as the lockdown for COVID began on 23 January 2020 and the slow rebound as Wuhan reopened on 9 April 2020. Daily updates of city-scale NO_x and CO₂ emissions provide policymakers with emission and policy control data on NO_x and CO₂ emission control in urban environments.

In the future, following the launch of the Carbon Dioxide Monitoring mission (CO2M) (Sierk et al., 2021), our improved superposition column method may be explored further to constrain city-scale CO₂ and NO_x emissions to assess the effectiveness of emission control measures. CO2M provides simultaneous and co-located CO₂ and NO₂ observations with a wider swath than OCO-2, providing better opportunities to verify and improve CO₂ and NO_x emissions from space.

Data availability. The S-5P TROPOMI v2.3.1 NO₂ column data is available from <https://data-portal.s5p-pal.com/cat-doc> (last access: 3, November 2022); the ERA5 data can be found at <https://cds.climate.copernicus.eu/cdsapp#!/dataset/reanalysis-era5-pressure-levels?tab=overview> (last access: 3, November 2022); the OCO-2 v10r XCO₂ data can be downloaded from https://disc.gsfc.nasa.gov/datasets/OCO2_L2_Lite_FP_10r/summary?keywords=CO2 (last access: 3, November 2022); The GEOS-Chem model simulated data is available on request (zhangqq@cma.gov.cn).

Author contributions. Q.Z. and K.F.B designed the research; Q.Z. performed the data analysis, model development and result validation. B.Z. and H.Z. provided the ABACAS-EI NO_x and CO₂ emission inventories. H.E. provided the 2.3.1 version of

TROPOMI tropospheric NO₂ product. C.C. provided MEIC NO_x emissions and performed the CMAQ simulations. X. Z. provided helpful discussions. Q.Z. and K.F.B. wrote the paper.

Competing interests. The authors declare no competing financial interest.

Acknowledgement. This work is funded by the National Natural Science Foundation of China (No.: 41805098) and the China
400 Scholarship Council (202005330023). Improvements in TROPOMI NO₂ data (v2.3.1) have received support from the KNMI
MSO NO₂NEXT project.

References

- Bauwens, M., Compernelle, S., Stavrou, T., Muller, J. F., van Gent, J., Eskes, H., Levelt, P. F., van der, A. R., Veeffkind, J. P., Vlietinck, J., Yu, H., and Zehner, C.: Impact of coronavirus outbreak on NO₂ pollution assessed using TROPOMI and OMI observations, *Geophys. Res. Lett.*, e2020GL087978, 10.1029/2020GL087978, 2020.
- 405 Beirle, S., Boersma, K. F., Platt, U., Lawrence, M. G., and Wagner, T.: Megacity emissions and lifetimes of nitrogen oxides probed from space, *Science*, 333, 1737-1739, 10.1126/science.1207824, 2011.
- Beirle, S. B., K.F., Platt, U., Lawrence, M.G., Wagner, T.: Megacity Emissions and Lifetimes of Nitrogen Oxides Probed from Space, *Science*, 333, 2011.
- 410 Berezin, E. V., Konovalov, I. B., Ciais, P., Richter, A., Tao, S., Janssens-Maenhout, G., Beekmann, M., and Schulze, E. D.: Multiannual changes of CO₂ emissions in China: indirect estimates derived from satellite measurements of tropospheric NO₂ columns, *Atmos. Chem. Phys.*, 13, 9415-9438, 10.5194/acp-13-9415-2013, 2013.
- Ding, J., A, R. J., Eskes, H. J., Mijling, B., Stavrou, T., Geffen, J. H. G. M., and Veeffkind, J. P.: NO_x Emissions Reduction and Rebound in China Due to the COVID-19 Crisis, *Geophys. Res. Lett.*, 47, 10.1029/2020gl089912, 2020.
- 415 Eskes, H., Van Geffen, J., Sneep, M., Veeffkind, J. P., Niemeijer, S., and Zehner, C.: S5P Nitrogen Dioxide v02.03.01 intermediate reprocessing on the S5P-PAL system: Readme file, 2021.
- Feng, S., Jiang, F., Wang, H., Wang, H., Ju, W., Shen, Y., Zheng, Y., Wu, Z., and Ding, A.: NO_x Emission Changes Over China During the COVID-19 Epidemic Inferred From Surface NO₂ Observations, *Geophys. Res. Lett.*, 47, e2020GL090080, 10.1029/2020GL090080, 2020.
- Griffin, D., McLinden, C. A., Boersma, F., Bourassa, A., Damers, E., Degenstein, D., Eskes, H., Fehr, L., Fioletov, V., Hayden, K., Kharol, S. K., Li, S. M., Makar, P., Martin, R. V., Mihele, C., Mittermeier, R. L., Krotkov, N., Sneep, M., Lamsal, L. N., Ter Linden, M., van Geffen, J., Veeffkind, P., Wolde, M., and Zhao, X.: High resolution mapping of nitrogen dioxide with TROPOMI: First results and validation over the Canadian oil sands, *Geophys. Res. Lett.*, 46, 1049-1060, 10.1029/2018GL081095, 2019.
- 420 Gunson M and Eldering, A.: OCO-2 Level 2 bias-corrected XCO₂ and other select fields from the full-physics retrieval aggregated as daily files, Retrospective processing V10r, Greenbelt, MD, USA, Goddard Earth Sciences Data and Information Services Center (GES DISC), last access: 31-05-2022, 10.5067/E4E140XDMPO2, 2020.
- 425 Hersbach, H., Bell, B., Berrisford, P., Hirahara, S., Horányi, A., Muñoz-Sabater, J., Nicolas, J., Peubey, C., Radu, R., Schepers, D., Simmons, A., Soci, C., Abdalla, S., Abellan, X., Balsamo, G., Bechtold, P., Biavati, G., Bidlot, J., Bonavita, M., Chiara, G., Dahlgren, P., Dee, D., Diamantakis, M., Dragani, R., Flemming, J., Forbes, R., Fuentes, M., Geer, A., Haimberger, L., Healy, S., Hogan, R. J., Hólm, E., Janisková, M., Keeley, S., Laloyaux, P., Lopez, P., Lupu, C., Radnoti, G., Rosnay, P., Rozum, I., Vamborg, F., Villaume, S., and Thépaut, J. N.: The ERA5 global reanalysis, *Q J R Meteorol Soc.*, 146, 1999-2049, 10.1002/qj.3803, 2020.
- 430 Hua, J., Zhang, Y., de Foy, B., Mei, X., Shang, J., and Feng, C.: Competing PM_{2.5} and NO₂ holiday effects in the Beijing area vary locally due to differences in residential coal burning and traffic patterns, *Sci. Total. Environ.*, 750, 141575, 10.1016/j.scitotenv.2020.141575, 2021.
- Huang, X., Ding, A., Gao, J., Zheng, B., Zhou, D., Qi, X., Tang, R., Wang, J., Ren, C., Nie, W., Chi, X., Xu, Z., Chen, L., Li, Y., Che, F., Pang, N., Wang, H., Tong, D., Qin, W., Cheng, W., Liu, W., Fu, Q., Liu, B., Chai, F., Davis, S. J., Zhang, Q., and He, K.: Enhanced secondary pollution offset reduction of primary emissions during COVID-19 lockdown in China, *Natl Sci Rev.*, 8, nwaal37, 10.1093/nsr/nwaa137, 2021.
- 435 Jacob, D.: Introduction to Atmospheric Chemistry, Princeton Univ. Press, 1999.
- Lamsal, L. N., Martin, R. V., Padmanabhan, A., van Donkelaar, A., Zhang, Q., Sioris, C. E., Chance, K., Kurosu, T. P., and Newchurch, M. J.: Application of satellite observations for timely updates to global anthropogenic NO_x emission inventories, *Geophys. Res. Lett.*, 38, n/a, 440 10.1029/2010gl046476, 2011.

- Lamsal, L. N., Martin, R. V., van Donkelaar, A., Celarier, E. A., Bucsela, E. J., Boersma, K. F., Dirksen, R., Luo, C., and Wang, Y.: Indirect validation of tropospheric nitrogen dioxide retrieved from the OMI satellite instrument: Insight into the seasonal variation of nitrogen oxides at northern midlatitudes, *J. Geophys. Res.*, 115, 10.1029/2009jd013351, 2010.
- 445 Li, K., Jacob, D. J., Shen, L., Lu, X., De Smedt, I., and Liao, H.: Increases in surface ozone pollution in China from 2013 to 2019: anthropogenic and meteorological influences, *Atmos. Chem. Phys.*, 20, 11423-11433, 10.5194/acp-20-11423-2020, 2020.
- Li, M., Zhang, Q., Kurokawa, J.-i., Woo, J.-H., He, K., Lu, Z., Ohara, T., Song, Y., Streets, D. G., Carmichael, G. R., Cheng, Y., Hong, C., Huo, H., Jiang, X., Kang, S., Liu, F., Su, H., and Zheng, B.: MIX: a mosaic Asian anthropogenic emission inventory under the international collaboration framework of the MICS-Asia and HTAP, *Atmos. Chem. Phys.*, 17, 935-963, 10.5194/acp-17-935-2017, 2017.
- 450 Liu, F., Beirle, S., Zhang, Q., Dörner, S., He, K., and Wagner, T.: NO_x lifetimes and emissions of cities and power plants in polluted background estimated by satellite observations, *Atmos. Chem. Phys.*, 16, 5283-5298, 10.5194/acp-16-5283-2016, 2016.
- Liu, F., Duncan, B. N., Krotkov, N. A., Lamsal, L. N., Beirle, S., Griffin, D., McLinden, C. A., Goldberg, D. L., and Lu, Z.: A methodology to constrain carbon dioxide emissions from coal-fired power plants using satellite observations of co-emitted nitrogen dioxide, *Atmos. Chem. Phys.*, 20, 99-116, 10.5194/acp-20-99-2020, 2020a.
- 455 Liu, M., Lin, J., Kong, H., Boersma, K. F., Eskes, H., Kanaya, Y., He, Q., Tian, X., Qin, K., Xie, P., Spurr, R., Ni, R., Yan, Y., Weng, H., and Wang, J.: A new TROPOMI product for tropospheric NO_x columns over East Asia with explicit aerosol corrections, *Atmos. Meas. Tech.*, 13, 4247-4259, 10.5194/amt-13-4247-2020, 2020b.
- Liu, Z., Ciais, P., Deng, Z., Davis, S. J., Zheng, B., Wang, Y., Cui, D., Zhu, B., Dou, X., Ke, P., Sun, T., Guo, R., Zhong, H., Boucher, O., Breon, F. M., Lu, C., Guo, R., Xue, J., Boucher, E., Tanaka, K., and Chevallier, F.: Carbon Monitor, a near-real-time daily dataset of global CO₂ emission from fossil fuel and cement production, *Sci. Data*, 7, 392, 10.1038/s41597-020-00708-7, 2020c.
- 460 Lorente, A., Boersma, K. F., Eskes, H. J., Veefkind, J. P., van Geffen, J., de Zeeuw, M. B., Denier van der Gon, H. A. C., Beirle, S., and Krol, M. C.: Quantification of nitrogen oxides emissions from build-up of pollution over Paris with TROPOMI, *Sci. Rep.*, 9, 20033, 10.1038/s41598-019-56428-5, 2019.
- ODell, C., Eldering, A., Gunson, M., Crisp, D., Fisher, B., Kiel, M., Kuai, L., Laughner, J., Merrelli, A., Nelson, R., Osterman, G., Payne, V., Rosenberg, R., Taylor, T., Wennberg, P., Kulawik, S., Lindqvist, H., Miller, S., and Nassar, R.: Improvements in XCO₂ accuracy from OCO-2 with the latest ACOS v10 product, EGU General Assembly 2021, online, 19–30 Apr 2021, EGU21-10484, 2021.
- 465 Qu, H.: Summertime ozone pollution over China: observations and simulations, Dissertation for the degree of Doctor of Philosophy, School of Earth and Atmospheric Science, Georgia Institute of Technology, 2020.
- Reuter, M., Buchwitz, M., Schneising, O., Krautwurst, S., O'Dell, C. W., Richter, A., Bovensmann, H., and Burrows, J. P.: Towards monitoring localized CO₂ emissions from space: co-located regional CO₂ and NO₂ enhancements observed by the OCO-2 and S5P satellites, *Atmos. Chem. Phys.*, 19, 9371-9383, 10.5194/acp-19-9371-2019, 2019.
- 470 Reuter, M., Buchwitz, M., Hilboll, A., Richter, A., Schneising, O., Hilker, M., Heymann, J., Bovensmann, H., and Burrows, J. P.: Decreasing emissions of NO_x relative to CO₂ in East Asia inferred from satellite observations, *Nature Geosci.*, 7, 792-795, 10.1038/ngeo2257, 2014.
- Riess, T. C. V. W., Boersma, K. F., van Vliet, J., Peters, W., Sneep, M., Eskes, H., and van Geffen, J.: Improved monitoring of shipping NO₂ with TROPOMI: decreasing NO_x emissions in European seas during the COVID-19 pandemic, *Atmos. Meas. Tech.*, 15, 1415-1438, 10.5194/amt-15-1415-2022, 2022.
- 475 Shah, V., Jacob, D. J., Li, K., Silvern, R. F., Zhai, S., Liu, M., Lin, J., and Zhang, Q.: Effect of changing NO_x lifetime on the seasonality and long-term trends of satellite-observed tropospheric NO₂ columns over China, *Atmos. Chem. and Phys.*, 20, 1483-1495, 10.5194/acp-20-1483-2020, 2020.
- Sierk, B., Fernandez, V., Bézy, J. L., Meijer, Y., Durand, Y., Bazalgette Courrèges-Lacoste, G., Pachot, C., Löscher, A., Nett, H., Minoglou, K., Boucher, L., Windpassinger, R., Pasquet, A., Serre, D., te Hennepe, F., Sodnik, Z., Cugny, B., and Karafolas, N.: The Copernicus CO2M mission for monitoring anthropogenic carbon dioxide emissions from space, International Conference on Space Optics — ICSO 2020, 10.1117/12.2599613, 2021.
- Statistics, W. B. o.: Statistical Bulletin on domestic economic and social development of Wuhan (2018), http://tjj.wuhan.gov.cn/tjfw/tjgb/202001/t20200115_841065.shtm (in Chinese, last access: 2022-05-19), 2019.
- 485 van Geffen, J., Boersma, K. F., Eskes, H., Sneep, M., ter Linden, M., Zara, M., and Veefkind, J. P.: S5P TROPOMI NO₂ slant column retrieval: method, stability, uncertainties and comparisons with OMI, *Atmos. Meas. Tech.*, 13, 1315-1335, 10.5194/amt-13-1315-2020, 2020.
- van Geffen, J., Eskes, H., Compernelle, S., Pinardi, G., Verhoelst, T., Lambert, J.-C., Sneep, M., ter Linden, M., Ludewig, A., Boersma, K. F., and Veefkind, J. P.: Sentinel-5P TROPOMI NO₂ retrieval: impact of version v2.2 improvements and comparisons with OMI and ground-based data, *Atmos. Meas. Tech.*, 15, 2037-2060, 10.5194/amt-15-2037-2022, 2022.
- 490 Visser, A. J., Boersma, K. F., Ganzeveld, L. N., and Krol, M. C.: European NO_x emissions in WRF-Chem derived from OMI: impacts on summertime surface ozone, *Atmos. Chem. Phys.*, 19, 11821-11841, 10.5194/acp-19-11821-2019, 2019.
- Wang, C., Wang, T., Wang, P., and Rakitin, V.: Comparison and Validation of TROPOMI and OMI NO₂ Observations over China, *Atmosphere*, 11, 10.3390/atmos11060636, 2020.
- 495 Zara, M., Boersma, K. F., Eskes, H., Denier van der Gon, H., Vilà-Guerau de Arellano, J., Krol, M., van der Swaluw, E., Schuch, W., and Velders, G. J. M.: Reductions in nitrogen oxides over the Netherlands between 2005 and 2018 observed from space and on the ground: Decreasing emissions and increasing O₃ indicate changing NO_x chemistry, *Atmos. Environ.: X*, 9, 10.1016/j.aeoa.2021.100104, 2021.

- Zhang, Q., Pan, Y., He, Y., Walters, W. W., Ni, Q., Liu, X., Xu, G., Shao, J., and Jiang, C.: Substantial nitrogen oxides emission reduction from China due to COVID-19 and its impact on surface ozone and aerosol pollution, *Sci. Total. Environ.*, 753, 142238, 10.1016/j.scitotenv.2020.142238, 2021.
- 500 Zhang, R., Zhang, Y., Lin, H., Feng, X., Fu, T.-M., and Wang, Y.: NO_x Emission Reduction and Recovery during COVID-19 in East China, *Atmosphere*, 11, 10.3390/atmos11040433, 2020.
- Zhao, B., Wang, S. X., Liu, H., Xu, J. Y., Fu, K., Klimont, Z., Hao, J. M., He, K. B., Cofala, J., and Amann, M.: NO_x emissions in China: historical trends and future perspectives, *Atmos. Chem. Phys.*, 13, 9869-9897, 10.5194/acp-13-9869-2013, 2013.
- 505 Zhao, B., Zheng, H., Wang, S., Smith, K. R., Lu, X., Aunan, K., Gu, Y., Wang, Y., Ding, D., Xing, J., Fu, X., Yang, X., Liou, K. N., and Hao, J.: Change in household fuels dominates the decrease in PM_{2.5} exposure and premature mortality in China in 2005-2015, *Proc. Natl. Acad. Sci. USA*, 115, 12401-12406, 10.1073/pnas.1812955115, 2018.
- Zhao, X., Zhou, W., and Han, L.: Human activities and urban air pollution in Chinese mega city: An insight of ozone weekend effect in Beijing, *Phys. Chem. Earth*, 110, 109-116, 10.1016/j.pce.2018.11.005, 2019.
- 510 Zheng, B., Zhang, Q., Geng, G., Shi, Q., Lei, Y., and He, K.: Changes in China's anthropogenic emissions during the COVID-19 pandemic [data set], figshare, Collection, <https://doi.org/10.6084/m9.figshare.c.5214920.v2>, 2021a.
- Zheng, B., Chevallier, F., Ciais, P., Broquet, G., Wang, Y., Lian, J., and Zhao, Y.: Observing carbon dioxide emissions over China's cities and industrial areas with the Orbiting Carbon Observatory-2, *Atmos. Chem. Phys.*, 20, 8501-8510, 10.5194/acp-20-8501-2020, 2020a.
- Zheng, B., Zhang, Q., Geng, G., Chen, C., Shi, Q., Cui, M., Lei, Y., and He, K.: Changes in China's anthropogenic emissions and air quality during the COVID-19 pandemic in 2020, *Earth Syst. Sci. Data*, 13, 2895-2907, 10.5194/essd-13-2895-2021, 2021b.
- 515 Zheng, B., Geng, G., Ciais, P., Davis, S. J., Martin, R. V., Meng, J., Wu, N., Chevallier, F., Broquet, G., Boersma, F., van der A, R. J., Lin, J., Guan, D., Lei, Y., He, K., and Zhang, Q.: Satellite-based estimates of decline and rebound in China's CO₂ emissions during COVID-19 pandemic, *Sci. Adv.*, 6, eabd4998, 2020b.
- Zheng, B., Geng, G., Ciais, P., Davis, S. J., Martin, R. V., Meng, J., Wu, N., Chevallier, F., Broquet, G., Boersma, F., van der A, R. J., Lin, J., Guan, D., Lei, Y., He, K., and Zhang, Q.: Satellite-based estimates of decline and rebound in China's CO₂ emissions during COVID-19 pandemic, *Sci. Adv.*, 6, 10.1126/sciadv.abd4998, 2020c.
- 520 Zheng, H., Zhao, B., Wang, S., Wang, T., Ding, D., Chang, X., Liu, K., Xing, J., Dong, Z., Aunan, K., Liu, T., Wu, X., Zhang, S., and Wu, Y.: Transition in source contributions of PM_{2.5} exposure and associated premature mortality in China during 2005-2015, *Environ. Int.*, 132, 105111, 10.1016/j.envint.2019.105111, 2019.